Effect of interface roughness on acoustic loss in tunable thin film bulk acoustic wave resonators

A. Vorobiev,[1,a)] J. Berge,[1] S. Gevorgian,[1] M. Löffler,[2] and E. Olsson[2]
[1]*Department of Microtechnology and Nanoscience, Chalmers University of Technology, SE-41296 Gothenburg, Sweden*
[2]*Department of Applied Physics, Chalmers University of Technology, SE-41296 Gothenburg, Sweden*

(Received 19 April 2011; accepted 11 June 2011; published online 29 July 2011)

Tunable 5.2 GHz bulk acoustic wave resonators utilizing $Ba_xSr_{1-x}TiO_3$ ferroelectric films with similar intrinsic properties but different interface roughness are fabricated and characterized. Increase in roughness from 3.2 nm up to 6.9 nm results in reduction in *Q*-factor from 350 down to 150 due to extrinsic acoustic losses caused by wave scattering at reflections from rough interfaces and other mechanisms associated with roughness. The increased roughness is a result of distortion of Pt bottom electrode caused by formation of heterogeneous enclosures of TiO_{2-x} in the Pt layer.
 [doi:10.1063/1.3610513]

I. INTRODUCTION

The tunable thin film bulk acoustic wave resonators (FBARs) based on DC field induced piezoelectric effect in paraelectric phase $Ba_xSr_{1-x}TiO_3$ (BSTO), allowing novel reconfigurable/adaptable microwave circuits, have been successfully demonstrated for the last few years.[1–4] However, the practical applications of the BSTO FBARs are hindered by their relatively low acoustic *Q*-factor resulting in low figure of merit, i.e., *Qf* product typically below 600 GHz.[4] Application of the FBARs in a ladder filter, for example, requires *Qf* product at least 2000 GHz.[5] Recently we developed BSTO FBARs with improved *Q*-factor revealing *Qf* product 1875 GHz.[6] The improvement is achieved via optimization of the BSTO film growth conditions leading to decrease in extrinsic acoustic losses associated with the film structural imperfections. Our analysis indicates that the BSTO film structural quality may be further improved by increasing the film growth temperature. However, simultaneously it results in a drastic increase in interface roughness and corresponding acoustic loss. A commonly accepted loss mechanism associated with roughness is wave scattering at reflections from rough interfaces.[5] It is assumed that in non-tunable AlN FBARs operating typically below 2 GHz the scattering loss is negligible since the typical interface roughness of tens of nanometers is far below the acoustical wavelength.[5,7] In this paper we demonstrate experimentally and by modeling that the loss caused by scattering at interfaces with roughness even less than 10 nm cannot be neglected in the BSTO FBARs operating at 5.2 GHz due to higher frequency and almost two times lower BSTO sound velocity. Studies of physical mechanisms dealing with the roughness of the FBAR interfaces are very limited. In Ref. 7 roughness of the AlN FBAR interfaces is associated with two processing related reasons: deposition of metal layers and chemical mechanical polishing of the Bragg reflector stack. In this paper we consider the physical phenomena responsible for roughness of the interfaces which are specific for BSTO FBARs due to relatively high growth temperature of the BSTO films.

II. EXPERIMENTAL DETAILS

The BSTO FBAR test structures are fabricated as solidly mounted resonators on silicon substrates with resistivity 20 kΩ·cm. Two different Bragg reflectors are used, one consisting of three SiO_2 and two W layers with thicknesses 280 and 240 nm, respectively, and another consisting of three pairs of SiO_2/HfO_2 layers with thicknesses 284/260 nm. A 100 nm thick Pt film is used as the bottom electrode with 10 nm thick W and 25/20 nm thick TiO_{2-x}/Ti adhesion layers for W and HfO_2 based Bragg reflectors, respectively. The TiO_x layer serves as a Ti diffusion barrier. The reflector and bottom electrode stacks are deposited by magnetron sputtering of metallic targets without substrate heating. The HfO_2 layers are deposited by reactive magnetron sputtering of a Hf target having 2.7% of Zr by weight. The 290 nm thick BSTO films are grown by rf magnetron sputtering of the $Ba_{0.25}Sr_{0.75}TiO_3$ target at set point temperature 585 °C. A patterned 100 nm thick Al film is used as a top electrode. Details of the design and fabrication of the FBAR test structures are described in Ref. 6. Permittivity of the BSTO films is calculated from capacitance measured at 1 MHz using an HP 4285 A LCR-meter. The complex input impedance $Z = \mathrm{Re}Z + \mathbf{j}\mathrm{Im}Z$ and admittance of the test structures are calculated using S_{11} parameters measured by an Agilent N5230 A vector network analyzer and GSG microprobes in the frequency range 1–10 GHz. The modified Butterworth-Van Dyke (MBVD) circuit model is used for deembedding of the electrical loss associated with series resistance R_s. The series resistance in the MBVD model is found as the real part of impedance at the high frequency limit. The series and parallel resonance frequencies f_s and f_p are defined as the frequencies corresponding to the maximum of the real part of the admittance and impedance, respectively. The *Q*-factors are evaluated at 25 V dc bias as

a)Electronic mail: andrei.vorobiev@chalmers.se.

$$Q = \frac{1}{2} f_s \frac{\partial \varphi}{\partial f}\bigg|_{f=f_s}, \quad (1)$$

where the phase angle is given as $\varphi = \arctan[\mathrm{Im}Z/(\mathrm{Re}Z\text{-}R_s)]$. The effective electromechanical coupling coefficient is evaluated using measured resonant frequencies:

$$k_t^2 = \frac{\pi f_s}{2 f_p} \cot\left(\frac{\pi f_s}{2 f_p}\right). \quad (2)$$

The FBAR and BSTO film parameters presented in the next section are results of averaging over nine test structures fabricated and measured on the same sample. Deviations of the resonance frequencies measured within each sample are less than 5 MHz which indicates high reproducibility of both fabrication and characterization processes. The W and HfO_2 based samples are fabricated in different runs. However, consistent dependencies of the parameters on the BSTO film growth temperature measured at a large number of samples (not presented in this paper) allows a conclusion about high run to run reproducibility also. The BSTO film of the HfO_2 based FBAR is removed by HF etching to study surface morphology of the Pt bottom electrode. The film surface is characterized using an atomic force microscope (AFM) Digital Instruments Dimension 3000 SPM operating in tapping mode. The surface roughness is evaluated using the SPIP 4.6.1.0 software tool as the root mean square (rms) parameter. Transmission electron microscopy (TEM) studies are conducted on a Tecnai G2 T20 ST microscope at 200 kV acceleration voltage, both in imaging and diffraction modes. Energy-dispersive x-ray spectroscopy (EDX) is performed on the Pt and HfO_2 layers in the TEM operating in scanning mode using the electron beam as a local probe.

III. RESULTS AND DISCUSSION

Figure 1 shows the reflection coefficients of the W and HfO_2 based Bragg reflectors calculated assuming acoustic waves incident from an infinitely thick ferroelectric layer.[8] The HfO_2 based Bragg reflectors reveal a narrower bandwidth due to the lower acoustic impedance of HfO_2 in comparison with that of W. However, the bandwidth of the HfO_2 based reflector is still more than sufficient for the BSTO FBAR applications. According to our simulations the difference in the reflection coefficients (see inset in Fig. 1) is negligible in the range of measured resonances.

Figure 2 shows the resonance frequency and Q-factor of the W and HfO_2 based FBARs versus dc bias voltage. The resonance frequency of both FBARs decreases with dc bias by approximately 1% at 25 V. The resonance frequency of the HfO_2 based FBAR is slightly higher which can be explained by reduced average thickness of the BSTO film caused by processing tolerances. The surface roughness of the BSTO films is 3.2 and 6.9 nm on the W and HfO_2 based reflectors, respectively. The Q-factors approach zero at low fields because of the nature of the field induced piezoeffect. It can be seen that the Q-factor of the HfO_2 based FBAR is significantly lower than that of the W FBAR (ca. 150 and 350, respectively, at 25 V). Below we show that this difference can be explained by extrinsic acoustic losses associated with interface roughness.

Figure 3 shows the permittivity of the BSTO films and the effective electromechanical coupling coefficient versus dc bias voltage for FBARs with W and HfO_2 based Bragg reflectors. The BSTO film grown on the latter reveals a 12% higher zero field apparent permittivity while its fractional tunability is only 3% higher. This indicates that the higher apparent permittivity can be associated partly with reduced average thickness of the BSTO film and mainly with increased effective electrode area due to rougher bottom and top interfaces. The effective coupling coefficients increase with dc bias from almost zero (Fig. 3) because the k_t^2 is proportional to a DC polarization.[9] One can expect a lower effective coupling coefficient of the HfO_2 based FBAR due to a substantial portion of acoustic energy stored in the near-in reflector area.[5] However, it is slightly higher which can be explained by higher DC field due to lower BSTO film average thickness caused by increased roughness. The fairly similar dielectric response of the BSTO films and the effective coupling coefficients of the W and HfO_2 based FBARs indicates that their BSTO intrinsic acoustic properties are similar as well.

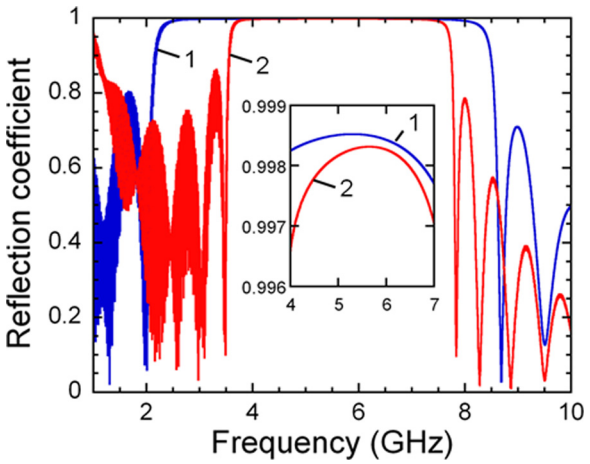

FIG. 1. (Color online) Simulated reflection spectra of the W (1) and HfO_2 (2) based reflector stacks. The zoomed inset shows the reflection coefficients near the resonant frequency.

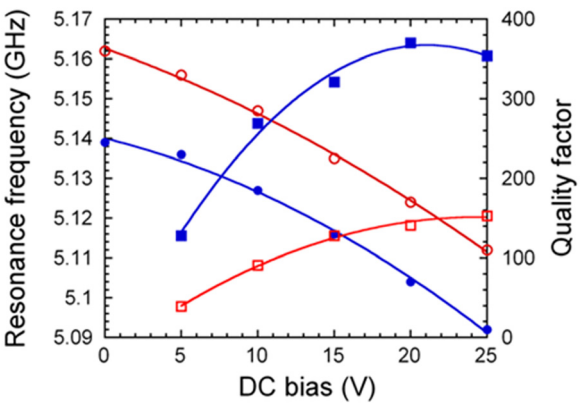

FIG. 2. (Color online) Resonance frequency (circles) and Q-factor (squares) of the W (closed symbols) and HfO_2 (open symbols) based FBARs vs dc bias voltage. The lines are polynomial curve fit.

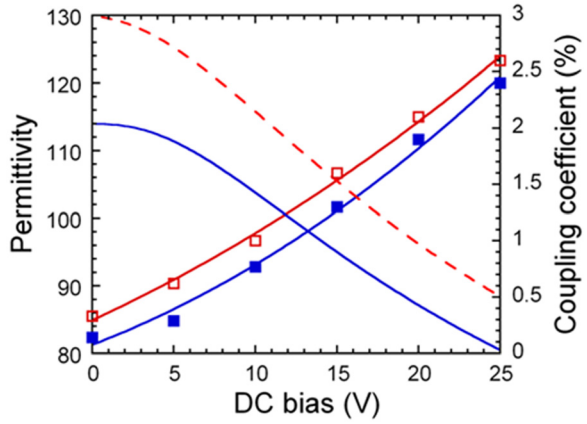

FIG. 3. (Color online) Permittivity and effective electromechanical coupling coefficient of the W (solid line and closed squares, respectively) and HfO_2 (dashed line and open squares, respectively) based FBARs vs dc bias voltage. The effective electromechanical coupling coefficient lines are polynomial curve fit.

Figure 4(a) and 4(b) shows AFM images of the BSTO films grown on W and HfO_2 based Bragg reflectors. It can be seen that the surface morphology of the BSTO film on the W based reflector is defined mainly by the tips of the columnar grains resulting in surface roughness of 3.2 nm. The BSTO film on the HfO_2 reflector reveals a larger surface roughness of 6.9 nm due to the formation of ridge-like features which, we assume, is a result of the deformation of the Pt bottom electrode. Figure 4(c) shows AFM image of the Pt film on HfO_2 based reflector after removing the BSTO film. The Pt film surface reveals ridges with roughness 14.9 nm. Figure 4(d) shows TEM cross section micrograph of the Pt bottom electrode on the HfO_2 based reflector. It can be seen that the Pt layer is heavily deformed and contains heterogeneous enclosures which we identified by EDX analysis as TiO_{2-x} grains. We assume that during high temperature growth of the BSTO film the excessive Ti from the not fully oxidized TiO_{2-x} layer diffuses intensively along the Pt columnar grain boundaries while oxygen is propagating in the opposite direction. Oxidation of Ti inside the Pt layer results in formation of TiO_{2-x} grains, volume expansion and deformation of the Pt electrode.[10] A similar but much less pronounced phenomenon we observe in the Pt with W adhesion layer on the W based Bragg reflector. The tungsten oxide secondary grains in the Pt are relatively small which does not lead to a remarkable Pt layer deformation and roughening of interfaces. Our explanation of this is based on the following arguments. The self-diffusion coefficient of W is ca. 3 times lower than that of Ti.[11] Gibbs-free energy of formation of titanium oxides is almost 2 times lower than that of the tungsten oxides.[12] Additionally the Pt layer on the HfO_2 based Bragg reflector is subjected to lower compressive stress than that on the W based one. The compressive stress, arising during heating up to the BSTO film growth temperature, is caused by lower thermal expansion of the Si substrate and the SiO_2 layers of the Bragg reflectors. However, the compressive stress in the Pt layer on HfO_2 based Bragg reflector is reduced by larger thermal expansion of the HfO_2 in comparison with that of the W (Table I). The reduced

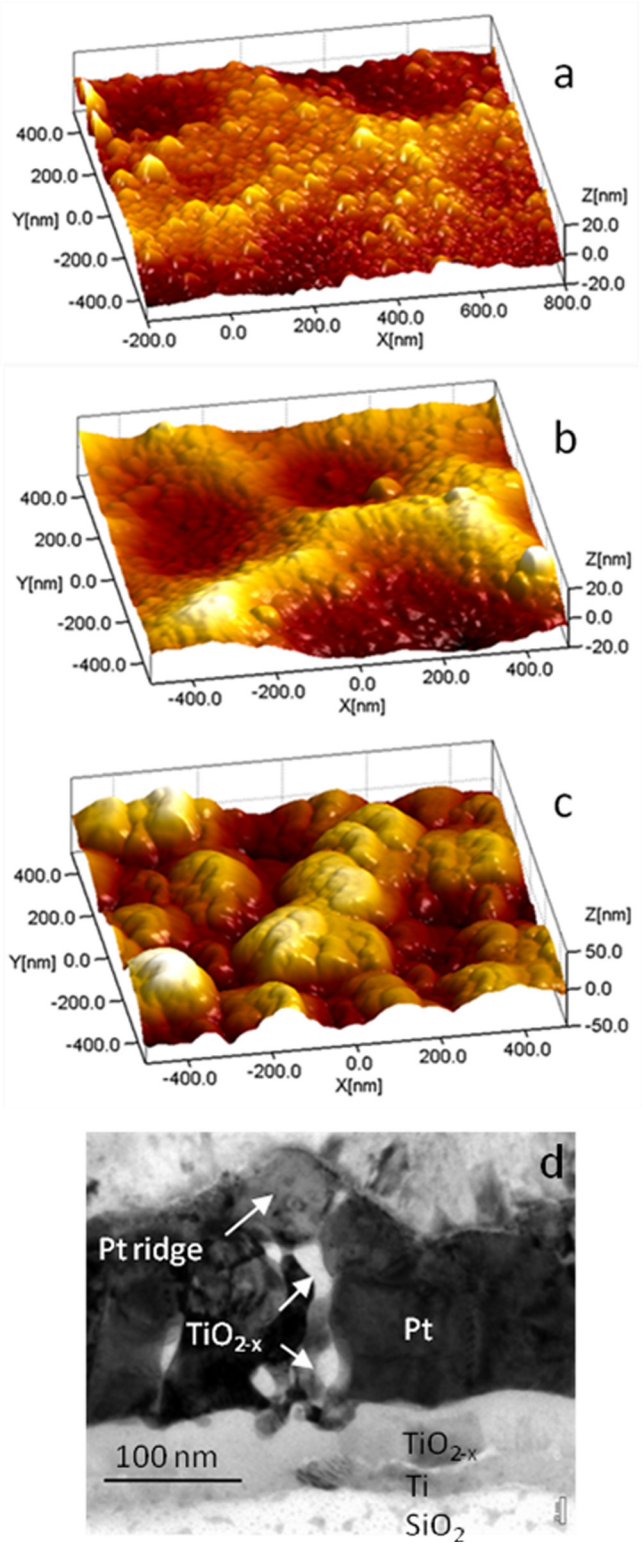

FIG. 4. (Color online) AFM images of the BSTO films grown on W (a) and HfO_2 (b) based Bragg reflectors; AFM image of the Pt film on HfO_2 based Bragg reflector after removing the BSTO film (c); TEM cross section micrograph of the Pt interface on HfO_2 based Bragg reflector (d).

compressive stress provides relatively open intergrain channels for the Ti and oxygen diffusion which results in enhanced formation of the TiO_{2-x} enclosures in the Pt layer.

The increased roughness at the interfaces of the BSTO FBAR on the HfO_2 Bragg reflector results in an increase in

TABLE I. Coefficients of thermal expansion ($\times 10^{-6}\,K^{-1}$).

Pt	SiO_2	W	HfO_2 (1.77% Zr)[a]	Si
8.8	0.5	4.5	9 (Ref. 13)	2.6

[a]Average content of Zr (in at. %) in the HFO2 films obtained by our EDX analysis.

the extrinsic acoustic losses due to several possible loss mechanisms. The commonly accepted mechanism of wave scattering at reflections from rough interfaces assumes redirection of vertically moving acoustic energy toward lateral directions. This causes the waves to leave the active resonator region and dissipate either in the device substrate or in the region surrounding the device laterally.[5] It can be seen from Fig. 4(d), that the surface of the SiO_2 layer (the main reflecting surface at the bottom interface) is relatively smooth. Therefore, we assume that the scattering loss is mainly defined by the Al top electrode roughness which is approximately the same as that of the BSTO film surface [Fig. 4(b)]. For a single reflection act and transverse roughness scale much smaller than the wavelength, the attenuation coefficient mainly depends on the roughness according to the formula[14]

$$\Gamma_R = 2\pi 8.68 q^2 \eta^2 \mathrm{dB}, \tag{3}$$

where q and η are the wave number and rms roughness, respectively. The attenuation coefficient then allows calculation of the Q-factor associated with wave scattering Q_R in accordance with its definition based on the ratio of the total energy to the power lost in a half-cycle. For the W based FBAR one can readily get $Q_R \approx 1240$ and for the HfO_2 based FBAR $Q_R \approx 262$. This difference indicates a domination of scattering loss in the total loss balance of the HfO_2 based FBAR. The $Q_R \approx 262$ is larger than the measured Q-factor (Fig. 2) because it does not take into account other loss mechanisms associated with roughness. In particular, we expect contribution of loss associated with shear waves generated by BSTO grains with tilted c axis.[6] Our studies indicate that the grain misalignment increases with roughness of the Pt bottom electrode. Besides we expect additional reduction of the Q-factor with roughness due to resonance broadening by local thickness variations. This effect assumes that the local film areas have the same acoustic and dielectric properties but different heights and thus closely spaced but different resonance frequencies. It results in broadening of the FBAR resonance curve and, hence, reduction in the overall Q-factor.[15] For the W based FBAR the calculated $Q_R \approx 1240$ is significantly higher than that measured $Q \approx 360$ because the interfaces are relatively smooth and the wave scattering at reflections from rough interfaces is not dominant loss mechanism. The other extrinsic loss mechanisms, including the generation of shear waves, Rayleigh scattering at localized defects, acoustic attenuation by interface amorphous layer etc., contribute to the total loss balance and reduce the Q-factor of the device under test.

In conclusion, we demonstrated that an increase in surface roughness of BSTO FBARs operating at 5.2 GHz from 3.2 up to 6.9 nm results in a decrease in the Q-factor from ca. 350 down to 150 due to extrinsic acoustic losses associated with interface roughness, mainly, wave scattering at reflections from rough interfaces. Additionally, we assume that the generation of shear waves by BSTO grains with tilted c-axis and resonance broadening by local thickness variations also contribute in decrease in the Q-factor with increase in roughness. In plans for the future we consider reduction of the roughness by an optimization of the diffusion barriers at the bottom interface and/or the control of compressive stress in the Pt bottom electrode layer.

ACKNOWLEDGMENTS

This work was supported by the project VR FBAR (2009-3460) of the Swedish Research Council.

[1]J. Berge, M. Norling, A. Vorobiev, and S. Gevorgian, J. Appl. Phys. **103**, 064508 (2008).
[2]A. Noeth, T. Yamada, P. Muralt, A. K. Tagantsev, and N. Setter, IEEE Trans. Ultrason. Ferroelectr. Freq. Control. **57**, 379 (2010).
[3]G. N. Saddik, D. S. Boesch, S. Stemmer, and R. York, IEEE MTT-S Int. Microwave Symp. Dig. **1**, 1263 (2008).
[4]X. Zhu, J. D. Phillips, and A. Mortazawi, IEEE MTT-S Int. Microwave Symp. Dig. **1**, 671 (2007).
[5]Ken-ya Hashimoto, *RF Bulk Acoustic Wave Filters for Communications* (Artech House, Norwood, MA, 2009).
[6]A. Vorobiev and S. Gevorgian, Appl. Phys. Lett. **96**, 212904 (2010).
[7]R. Thalhammer, J. Kaitila, R. Aigner, and S. Marksteiner, Proc. IEEE Ultrason. Symp. **1**, 282 (2004).
[8]D. A. Berlincourt, D. R. Curran, and H. Jaffe, in *Physical Acoustics*, edited by W. P. Mason (Academic, New York, 1964), Vol. 1, part A.
[9]A. Noeth, T. Yamada, V. O. Sherman, P. Muralt. A. K. Tagantsev, and N. Setter, J. Appl. Phys. **102**, 114110 (2007).
[10]M. Aspelmeyer, U. Klemradt, W. Hartner, H. Bachhofer, and G. Schindler, J. Phys. D: Appl. Phys. **34**, A173 (2001).
[11]B. Jacobsen, Q.-Z. Yin, D. Tinker, C. E. Lesher, *37th Annual Lunar and Planetary Science Conf.*, abstract no. 2410 (2006).
[12]A.-M. Azad and S. A. Akbar, Proc. of Optics East SPIE Conf. on Sensors for Harsh Environment, I. I. **5998**, 1 (2005).
[13]S. R. Skaggs, *Zero and Low Coefficient of Thermal Expansion Polycrystalline Oxides* (Los Alamos Scientific Laboratory, Los Alamos, 1977).
[14]S. G. Alekseev, G. D. Mansfel'd, N. I. Polzikova, and I. M. Kotelyanskii, Acoust. Phys. **53**, 465 (2007).
[15]J. Berge, A. Vorobiev, W. Steichen, and S. Gevorgian, IEEE Microwave Wireless Comp. Lett. **17**, 655 (2007).